Journal of Electroanalytical Chemistry 660 (2011) 85–90

Contents lists available at ScienceDirect

Journal of Electroanalytical Chemistry

journal homepage: www.elsevier.com/locate/jelechem

Search for multi-functional catalysts: The electrooxidation of acetaldehyde on Platinum–Ruthenium–Rhodium electrodeposits

Gisele A.B. Mello [a], M. Janete Giz [a], Giuseppe A. Camara [a,*], Alexandre Crisci [b], Marian Chatenet [c]

[a] Departamento de Química/UFMS, C.P. 549, 79070-900 Campo Grande, MS, Brazil
[b] Siences et Ingénerie des Matériaux et Procédés, SIMAP, UMR 5266 CNRS/Grenoble-INP/UJF, BP75, 38402 St. Martin d'Hères, France
[c] Laboratoire d'Electrochimie et de Physicochimie des Matériaux et des Interfaces, LEPMI, UMR 5279 CNRS/Grenoble-INP/UJF/UdS, BP75, 38402 St. Martin d'Hères, France

ARTICLE INFO

Article history:
Received 15 December 2010
Received in revised form 21 April 2011
Accepted 7 June 2011
Available online 15 June 2011

Keywords:
Acetaldehyde electrooxidation
Platinum–Ruthenium–Rhodium
Ethanol electrooxidation
FTIR *in situ*
Electrocatalysis

ABSTRACT

Preliminary studies on the influence of Platinum–Rhodium electrodeposits upon the rate of acetaldehyde electrooxidation showed that Rhodium plays a dual role during electrooxidation, because it favors the break of C–C bonds whilst prevents the deliverance of oxygen-containing species, thus inhibiting the oxidation steps. Based on these results, in this work Platinum–Ruthenium and Platinum–Ruthenium–Rhodium electrodeposits were prepared and characterized by electrochemical and spectroscopic methods (FTIR *in situ*). The addition of Ruthenium is justified by its ability to promote a facile oxidation of adsorbed species by activation of water molecules. The results indicate a compromise between the existence of superficial sites able to break carbon chains (provoked by Rhodium) and responsible by the oxidation of adsorbed species (provoked by Ruthenium). Among the atomic compositions investigated, PtRuRh (73:23:04) shows the maximum activity towards acetaldehyde electrooxidation, but the production of acetic acid seems to be the main responsible for this activity.

1. Introduction

The complete electrooxidation of acetaldehyde to carbon dioxide with high energetic yields would be considered a remarkable achievement in electrocatalysis, because acetaldehyde is formed on Platinum-based surfaces as the main product of electrooxidation of ethanol [1–4], provoking the waste of great part of the energetic content of the process and making direct ethanol fuel cell systems impracticable from both economical and technical points of view. As an attempt to overcome this difficulty, the number of studies concerning the electrooxidation of acetaldehyde has increased in the last few years [5–14]. Owing to the efforts of different research groups, some important characteristics are already known. For instance, for Platinum electrocatalysts it has been demonstrated that (i) acetaldehyde decomposes into adsorbed CO at potentials as low as 0.06 V [5], (ii) its adsorption also generates chemisorbed CH species [6], and (iii) the breaking of the C–C bond is easier in acetaldehyde than in ethanol [6]. Despite the recent advances into the understanding of the electrooxidation mechanism, the effective scission of C–C bonds in acetaldehyde, as in ethanol, continues to be a major problem in electrocatalysis. Surpassing this challenge requires intensive research devoted to the design of new materials with multi-functional characteristics, responsible for the steps of adsorption, fragmentation and oxidation of such molecules.

In this context, Rhodium has been considered as a suitable catalyst to promote the scission of C–C bonds during the electrooxidation of molecules like ethanol [15] and 2-propanol [16]. Based on these observations, we recently investigated the electrooxidation of acetaldehyde on electrodeposits of Platinum–Rhodium in several atomic compositions [14]. The results suggest that Rhodium helps to break C–C bonds, but fails as a multi-functional catalyst, because it prevents the activation of water necessary to promote subsequent oxidation steps [14]. The global outcome are materials with poorer activity than Platinum towards acetaldehyde electrooxidation.

As an attempt to overcome this difficulty here we report the influence of the atomic composition of Platinum–Ruthenium and Platinum–Ruthenium–Rhodium electrodeposits (from now onwards designed as PtRu and PtRuRh) on acetaldehyde electrooxidation in acidic media. Ru was chosen as a co-catalyst due to its ability to promote the oxidation of adsorbed species by activation of water molecules [11]. The electrodeposits were characterized by electron-probe microanalysis (EPMA) and investigated by electrochemical and *in situ* FTIR techniques.

2. Experimental

Solutions were prepared with Milli-Q water (18.2 MΩ cm^{-1}), $HClO_4$ (Suprapur, Merck) and CH_3CHO (P.A., Merck). Before the

* Corresponding author. Tel.: +55 67 3345 3576; fax: +55 67 3345 3552.
E-mail address: giuseppe.silva@ufms.br (G.A. Camara).

1572-6657
doi:10.1016/j.jelechem.2011.06.009

measurements solutions were thoroughly purged with N_2. All the experiments were performed at room temperature (25.0 ± 1.0 °C).

The counter electrode was a Platinum sheet and all the potentials were measured against a reversible hydrogen electrode (RHE) in the same electrolyte.

The electrodeposits were prepared by electrochemical reduction of Rh^{3+}, Ru^{3+} and Pt^{4+}, at different atomic compositions obtained from $RhCl_3$, $RuCl_3$ and H_2PtCl_6 aqueous solutions, in 0.1 mol dm^{-3} $HClO_4$ and 0.05 V vs. RHE, during 5 min. PtRu and PtRuRh catalysts were electrodeposited either on a polished gold disk (0.78 cm^2 of geometric area) for FTIR experiments or on a gold foil (~0.5 cm^2) for cyclic voltammetry. Two series of electrodeposits were prepared. The first series consisted of binary PtRu catalysts ranging from 5 to 32 at% of Ru, whilst the second one consisted of PtRuRh electrodeposits. In this case, Pt was kept as the major component (compositions ranging 65–76 at%), whilst the composition of RuRh was varied from 23:04 to 03:32 at%.

The compositions of the electrodeposits were determined by EPMA, performed on a CAMECA SX50 microprobe. The measurements were performed at different accelerating voltages (7 and 10 kV) in order to vary the sampled depth through the deposited layers and the gold substrate. At each accelerating voltage, 10 points have been acquired to obtain for each element the intensity I_x of the characteristic wavelength (*i.e.* corresponding to Ru Lα, Rh Lα, Pt Mα and Au Lβ), rationed to the intensity obtained on pure standards I_{std} of the corresponding metals. It is wise noting that successive acquisitions were not measured at similar position on the sample to avoid contamination under the electron beam. Compositions and mass thickness were determined by analyzing the evolution of intensity ratio I_x/I_{std} versus the voltage, using the software Stratagem™ (see Table 1). In that process, one needs to consider that the deposit are homogeneous over the whole sample surface (in terms of thickness, composition and density), which is likely for electrodeposited layers.

The EPMA characterizations also enabled determining the physical thickness of the electrodeposits, *i.e.* the thickness of a non-porous layer, the density of which was recalculated from the at% determined from the elemental analysis.

Once obtained, the electrodeposits were characterized in 0.1 mol dm^{-3} $HClO_4$ by cyclic voltammetry in the potential range of 0.05–0.80 V vs. RHE at 20 mV s^{-1}. For the estimation of the real surface area, the electrodes were saturated with carbon monoxide by bubbling the gas for 10 min at 0.05 V vs. RHE in the solution containing only 0.1 mol dm^{-3} $HClO_4$. The excess of CO was then eliminated from the solution by bubbling pure N_2 for 10 min and cyclic voltammograms were recorded at 20 mV s^{-1} in the same potential range. The first cycle provided the total charge of CO oxidation, whilst a second one was taken to check the recovering of the original voltammetric profile. Before each experiment, the electrodes were dipped in hot H_2SO_4 and washed with Milli-Q water.

All the experiments were performed in triplicate. For the electrooxidation of acetaldehyde the potential was kept at 0.05 V and acetaldehyde was admitted in the cell to reach the concentration of 0.2 mol dm^{-3} and a new voltammetric cycle was obtained. Chronoamperometric experiments were performed in triplicate by monitoring the current–time response after application of a potential step. In order to obtain *i–t* curves, the electrodes were kept at 0.05 V in 0.1 mol dm^{-3} $HClO_4$ + 0.2 mol dm^{-3} CH_3CHO. Next, a potential step from 0.05 to 0.6 V was applied and the electrocatalytic activity was evaluated by measuring the current after 20 min.

In situ FTIR measurements were carried out by using a FTIR spectrometer equipped with a MCT detector. The counter electrode was a Platinum sheet. The experiments were made in the presence of 0.1 mol dm^{-3} $HClO_4$ + 0.2 mol dm^{-3} CH_3CHO. Reflectance spectra were collected as the ratio (R/R_o) where R represents a spectrum at a given potential and R_o is the spectrum collected at 0.05 V. Positive and negative bands represent the consumption and production of substances, respectively [17]. Spectra were computed from the average of 32 interferograms. The spectral resolution was set to 4 cm^{-1}. Details of the spectroelectrochemical cell and setup can be consulted in [17]. The electrochemical IR cell was fitted with a CaF_2 planar window for the collection of bands corresponding to the formation of CO_2 and acetic acid.

3. Results and discussion

3.1. Surface characterization of the electrodeposits

Table 1 summarizes the results of EPMA analyses performed for the various electrodeposited samples. For all, the mass thickness is on the order of 77 ± 12 μg cm^{-2}, the extreme values being 58 and 103 μg cm^{-2}. The at% non-negligibly differ from the nominal composition, but the trend is maintained for all samples. The corresponding wt% enabled the calculation of the practical bulk density for each electrodeposit, assuming the values for pure Pt, Ru and Rh (21.45, 12.2 and 12.4 g cm^{-3}, respectively). Combining these values and those of the mass thickness, one obtains the physical thickness, *i.e.* the thickness of a purely non-porous electrodeposited layer. The corresponding values are on the order of 38.6 ± 5.6 nm (the extreme values being 30.2 and 50.7 nm), which demonstrates that the gold surface is fully covered by the electrodeposits, as the voltammetric characterizations of Section 3.2. will confirm.

Although powerful to characterize the composition of the electrodeposited samples, EPMA cannot provide any insight regarding the crystallographic nature of the samples. For that purpose X-ray diffraction (XRD) would be a better tool. However, due to the very small thickness of the electrodeposits combined with the nanosize of the crystals/structures (observed from scan-

Table 1
Measured mass thickness and composition of the various electrodeposited samples; Corresponding calculated bulk density and physical thickness (*i.e.* thickness of a purely non-porous layer) of the electrodeposits.

Sample	Mass thickness/μg cm^{-2}	Composition/wt%				Composition/at%				Bulk density/g cm^{-3}	Physical thickness/nm
		Pt	Ru	Rh	Total	Pt	Ru	Rh	Total		
PtRu-50:50	71	78.2	19.03	–	97.2	68.0	32.0	–	100	19.1	37.2
PtRu-60:40	78	83.0	14.8	–	97.7	74.4	25.6	–	100	19.6	39.8
PtRu-70:30	103	89.8	8.7	–	98.5	84.3	15.7	–	100	20.3	50.7
PtRu-80:20	89	94	6.9	–	100. 9	87.6	12.4	–	100	21.0	42.4
PtRu-90:10	72	97.7	2.7	–	100.4	95.0	5.0	–	100	21.3	33.8
PtRuRh-60:35:5	79	83.6	13.5	2.1	99.2	73.5	23.0	3.5	100	19.8	39.8
PtRuRh-60:30:10	70	84.6	11.0	4.8	100.5	73.6	18.5	7.9	100	20.1	34.8
PtRuRh-60:25:15	72	84.4	7.9	5.8	98.0	76.3	13.7	10.0	100	19.8	36.4
PtRuRh-60:15:25	83	85.5	5.0	9.3	99.8	75.8	8.5	15.7	100	20.1	41.3
PtRuRh-60:5:35	58	77.0	2.0	20.0	99.0	64.9	3.2	31.9	100	19.2	30.2

ning electron-microscopy, not shown for brevity) one understands that the success of such XRD characterization is highly improbable. Nevertheless, as will be shown in the next section, electrochemistry can also provide insights about the degree of alloying of the metals.

3.2. Voltammetric characterization of PtRuRh electrodeposits in acidic media

As the voltammetric profiles of PtRu electrodeposits were already described in detail in previous papers of our group [18,19], the corresponding results will be not presented here. Shortly, PtRu electrodeposits show the typical behavior in acidic media: The peaks for H-adsorption are better defined as the Pt content increases, whilst currents in the double layer region grow with the Ru content. This latter feature is associated with the production of Ru oxides, which coincides with the occurrence of capacitive currents at Pt [18]. Moreover, the profiles correspond to PtRu alloyed surfaces more than to the coexistence of segregated Pt and Ru domains (the features characteristic to Pt facets are not well developed) [20].

The voltammetric characteristics of PtRuRh electrodeposits are depicted in Fig. 1. For purposes of comparison the PtRu (74:26) composition was also included. We observed that when the surface is enriched with Rh the adsorption–desorption hydrogen peaks are better defined. These results show a tendency similar to that previously observed by Gupta and Datta for PtRh electrodeposits in acidic media [21] and for PtRh carbon supported catalysts [22]. Also, the double layer region suffers a progressive diminution when the Rh content increases. This lowering of the pseudo-capacitive currents can be explained by the progressive diminution of Ru on the surface, which dislocates the production of superficial oxides for potentials not accessible in the present setup, since we are limiting the vertex potential to 0.8 V. As for the PtRu samples, these results are consistent with the presence of alloyed surfaces.

3.3. The catalytic activity as a function of the composition of the electrodeposits

To estimate the influence of the composition of the electrodeposits on the acetaldehyde electrooxidation, a series of chronoamperometric experiments was performed. For this, the working electrodes remained polarized at 0.05 V in a solution containing 0.2 mol dm^{-3} acetaldehyde + 0.1 mol dm^{-3} $HClO_4$. Subsequently, the potential was stepped to 0.6 V and the electrodes remained at this potential for additional 20 min. For each composition, three experiments were performed. Some representative current–time curves for both series are shown in Fig. 2. The values of the current density refer to the estimated real surface area. All catalysts present a continuous decay in activity, as already observed for PtRu deposits in presence of ethanol [18]. Next, values of the current density for acetaldehyde oxidation measured after 20 min were collected and plotted against the electrode composition. The corresponding results for binary (PtRu) and ternary (PtRuRh) electrodeposits are shown in Fig. 3a and b, respectively.

Despite the uncertainty of the currents (see the magnitude of the error bars) the electrodes with low Ru content exhibit a very low activity towards acetaldehyde oxidation (Fig. 3a). The curve exhibits a steep increase for compositions above 12 at% Ru. After

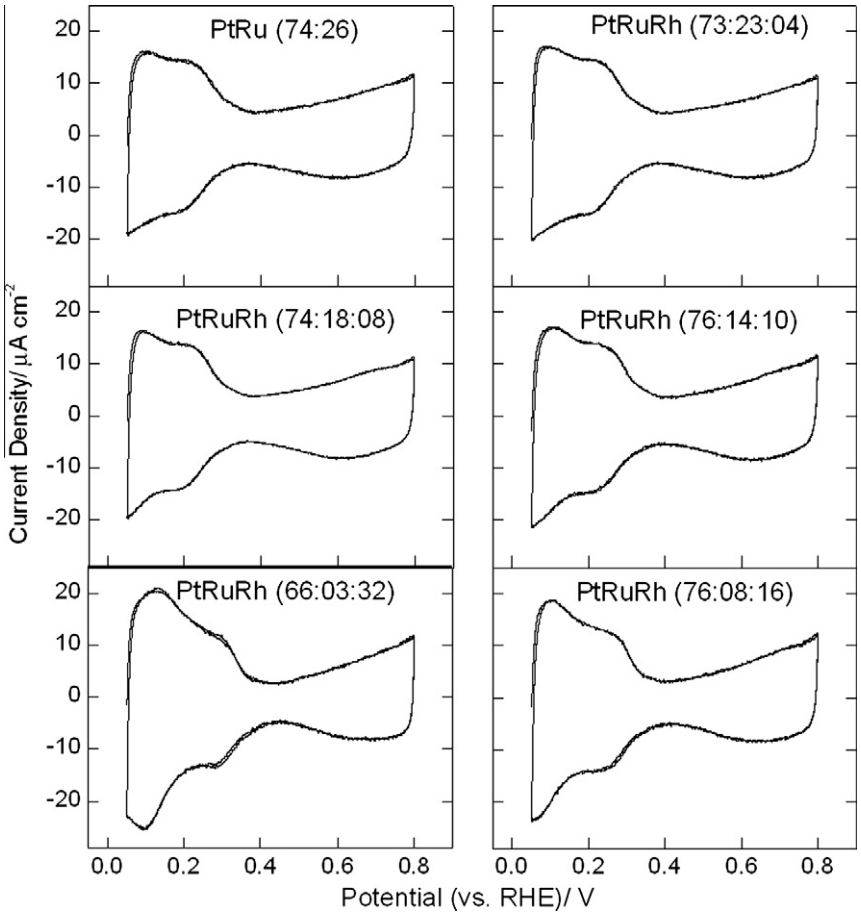

Fig. 1. Cyclic voltammograms of PtRuRh electrodeposits in 0.1 mol dm^{-3} $HClO_4$ at 25 °C. υ = 20 mV s^{-1}. Real atomic compositions indicated in the figure.

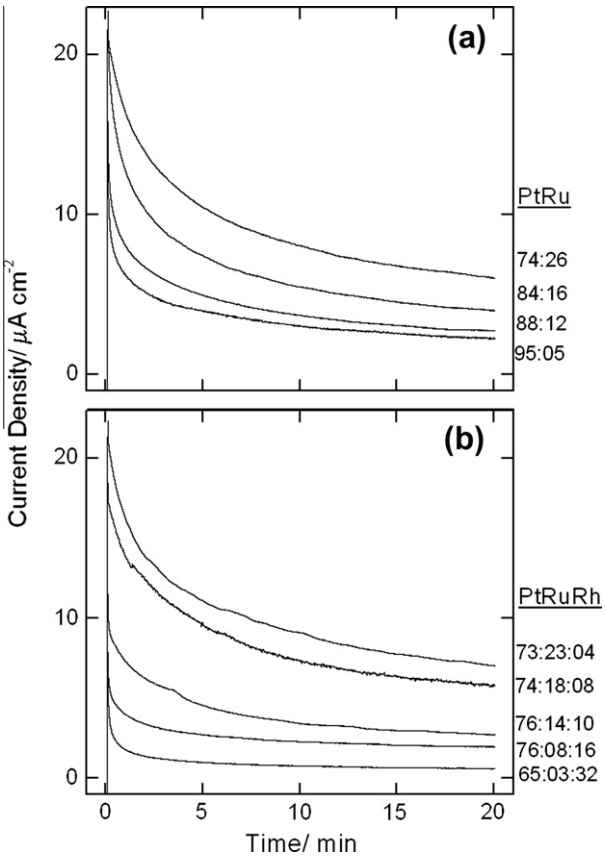

Fig. 2. Chronoamperograms for (a) PtRuRh and (b) PtRu electrodeposits after application of a potential step from 0.05 V to 0.6 V in 0.2 mol dm^{-3} CH_3CHO + 0.1 mol dm^{-3} $HClO_4$. Atomic compositions indicated in the figure. T = 25 °C.

a narrow maximum (~26 at% Ru), the activity presents a sharp decay for 32 at% Ru. This result is in line with previous observations made for PtRu electrodeposits in presence of ethanol, where PtRu atomic compositions around 70:30 showed the maximum activity during the electrooxidation of the alcohol [18]. Based on these results we decided to keep Pt as the major component (60 at% forecast, *i.e. ca.* 75 at% in practical, seems to be the minimum amount of Pt required to promote the adsorption of organic molecules at a reasonable rate), whilst the composition of RuRh was varied from (35:05) to (10:30) at% forecast, which corresponds to (23:04) to (03:32) at% in practical (see Table 1).

Fig. 3b shows the quasi-stationary currents as a function of Rh content for ternary electrodeposits. PtRu (74:26) is indicated by an arrow and is present at both sides of the figure. When Ru is replaced by *ca.* 4 at% of Rh it seems to be a small increase in the activity (in this case the differences are not statistically significant), whilst any further enrichment with Rh is detrimental to the electrooxidation process. With the aim to correlate the behavior shown in Figs. 2 and 3 with the reaction pathways established during the electrooxidation process we used *in situ* FTIR spectroscopy. Results are presented in the next section.

3.4. Following the production of CO_2 and acetic acid

Fig. 4 shows a series of FTIR spectra at 0.6 V collected during the electrooxidation of acetaldehyde for seven representative compositions of PtRu and PtRuRh. For purposes of comparison, the magnitudes of the spectra were normalized by the corresponding areas estimated from the CO-stripping procedure. Bands relative to the production of CO_2 (2343 cm^{-1}), and acetic acid (1280 cm^{-1}) are observed for all catalysts. Moreover, a weak feature referring to linearly adsorbed CO can be discriminated at ~2042 cm^{-1}, but, as already observed by Iwasita and co-workers, the use of electrodeposited surfaces reduces the band intensities for adsorbed species [23]. According to the authors, the reason for this effect probably originates from the rough structure of such surfaces [23]. Therefore, we did not attempt to establish any correlation between the CO band intensity and the capability of PtRu and PtRuRh deposits to adsorb and dissociate acetaldehyde. Band intensities for soluble species, on the other hand, do not present this problem and

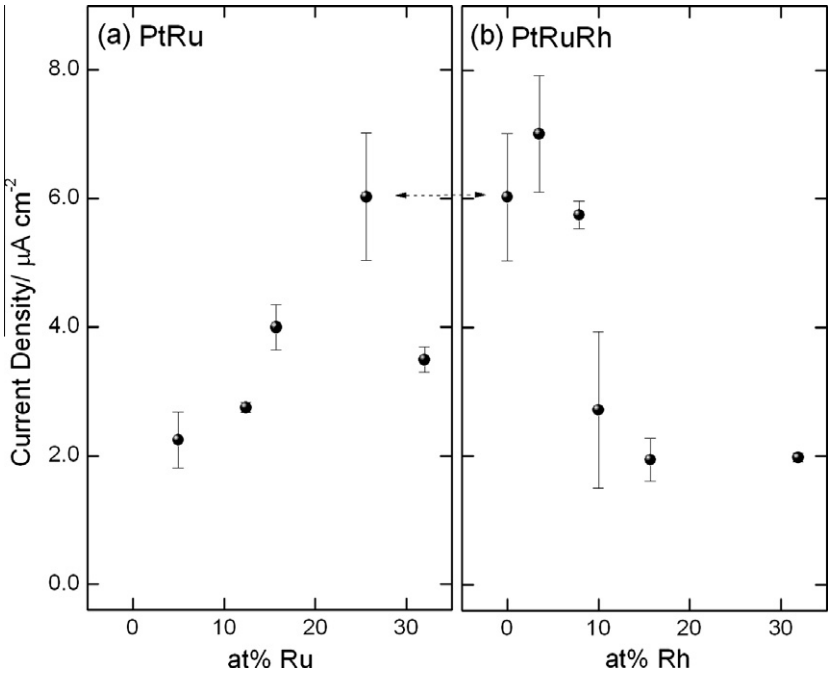

Fig. 3. Activity towards acetaldehyde electrooxidation as a function of (a) PtRu and (b) PtRuRh compositions. The data were obtained from *i*–*t* curves after 20 min of polarization at 0.6 V in 0.2 mol dm^{-3} CH_3CHO + 0.1 mol dm^{-3} $HClO_4$.

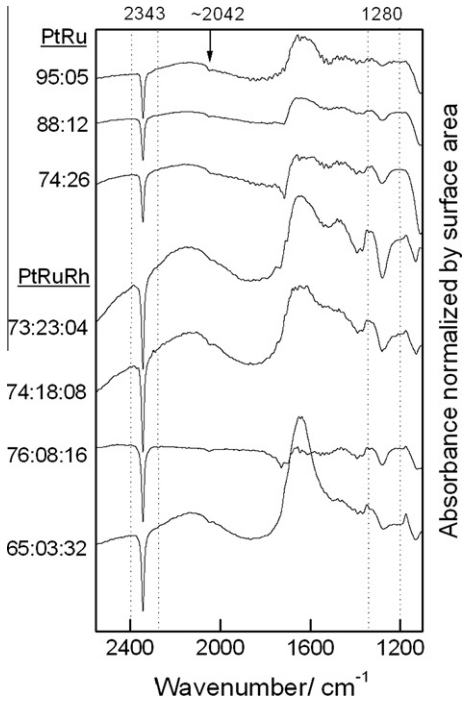

Fig. 4. *In situ* FTIR spectra for PtRu and PtRuRh in 0.2 mol dm^{-3} CH_3CHO + 0.1 mol dm^{-3} $HClO_4$. Reference spectra taken at 0.05 V. Sample spectra collected at 0.6 V during a linear sweep voltammogram. $\upsilon = 1$ mV s^{-1}. The nature of the catalyst and the real atomic compositions are indicated in the figure.

their production can be inferred from the corresponding band intensities.

Comparing the band intensities relative to the production of CO_2 and acetic acid, the following features are noteworthy:

(i) Fig. 4 (top) – when the binary electrodeposits are enriched with Ru, the CO_2 signal is virtually unaffected, whilst the production of acetic acid is clearly favored at PtRu (74:26) if compared with PtRu (95:05). The comparison of these data with Fig. 3a suggests that the gain in catalytic activity observed for PtRu (74:26) is probably associated to a higher production of acetic acid. These results are similar to those obtained for the electrooxidation of ethanol [3] and indicate that PtRu catalysts are not able to promote the scission of the C–C bond, which justifies the use of Rh as a co-catalyst at a first glance.

(ii) Fig. 4 (bottom) – For PtRuRh (73:23:04), both the production of acetic acid and CO_2 are enhanced if compared to PtRu (74:26) and suggest that the minor differences in the currents in Fig. 3a are probably due to higher oxidation rates concerning both pathways. For compositions richer in Rh the formation of acetic acid seems to be sensibly inhibited, whilst CO_2 signals are barely affected.

A more informative way to see these differences could be attained by plotting the ratio between the absorbances of CO_2 and acetic acid ($R_{C/H}$) at a certain potential (e.g., 0.6 V). However, we must remember that there is an intrinsic difficulty to follow the emergence of spectroscopic signals in thin layer configuration, because the bands are due to the production and accumulation of substances inside the thin layer [24–26]. In other words, any substance which was produced at lower potentials remains inside the thin layer during long periods of time and those moieties are added to the signals emerging from different potentials. In the present case, an additional difficulty is the fact that CO_2 is in gaseous phase, whilst acetic acid is a liquid at the experimental conditions

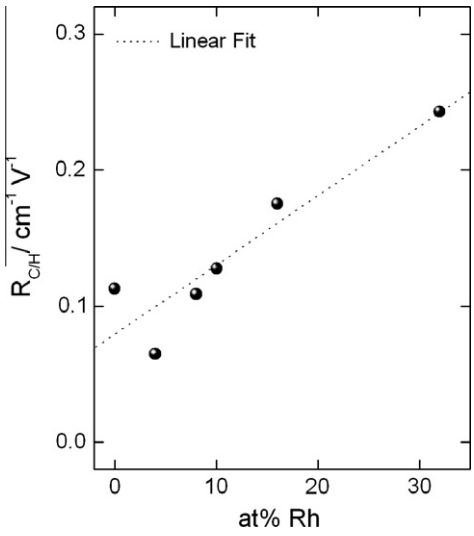

Fig. 5. Ratio of CO_2/acetic acid integrated absorbances ($R_{C/H}$) as a function of Rh atomic content. The values of A_c and A_H were extracted from FTIR spectra like those showed in Fig. 4 and calculated between the potentials of 0.55 and 0.6 V.

adopted. Thus, we must expect that the diffusion coefficients be significantly different for both substances and strongly influence the pure absorbance signal taken at a specific potential. Keeping this reasoning in mind, we subtract the absorbancies calculated at 0.6 V from those obtained at the previous potential where the spectra were collected (viz. 0.55 V), according to Eq. (a):

$$R_{C/H} = \frac{[A_C\ (0.6\ V) - A_C(0.55\ V)]}{[A_H(0.6\ V) - A_H(0.55)]} \quad (a)$$

where A_C and A_H stand for the CO_2 and acetic acid absorbances, respectively. The results for six illustrative compositions are depicted in Fig. 5.

$R_{C/H}$ shows a nearly linear increase with the Rh content (Fig. 5). If these results are compared with Fig. 4, it is evident that although the production of CO_2 can be accelerated in the presence of Rh (by a little amount), the ratio increases mainly due to the inhibition of the acetic acid production.

The optimum compromise between the existence of Rh superficial sites able to break carbon chains and Ru sites responsible for the oxidation of adsorbed species seems to be reached for PtRuRh (73:23:04). Consequently, this composition presents the higher global activity for acetaldehyde electrooxidation (Figs. 2 and 3b). As Ru is progressively replaced by Rh, the CO_2 pathway is barely affected, but the production of acetic acid is strongly inhibited (Fig. 4). Apparently, two effects (both caused by Rh) seem to inhibit the acetic acid pathway, namely, the enhanced ability to break C–C bonds and the increasing difficulty to donor oxygen-containing species [14].

If we take into account that acetic acid is the major responsible for the global charge involved in the electrooxidation of acetaldehyde [9,14], it becomes evident that a high catalytic activity has no direct connection with a higher selectivity towards CO_2 pathway, because the production of CO_2 seems to be not enough to replenish the loss of charge caused by the (relative) absence of acetic acid.

4. Conclusions

– The catalytic activity of PtRuRh towards the acetaldehyde oxidation is sensibly dependent on the composition of the electrodeposit. Current–time curves measured at several electrode compositions show an optimum PtRuRh composition of *ca.* (73:23:04) at%.

- The best global activity observed for PtRuRh (73:23:04) does not correspond to an expressive increase in the rate of CO_2 production. On the contrary, acetic acid production is favored at this composition.
- At relative high contents of Rh the increase on the production of CO_2 is insufficient to replenish the loss of charge caused by the inhibition of the acetic acid pathway. Consequently, the catalytic activity is lowered.

Acknowledgements

The authors thank CNPq (process 576742/2008-2), FUNDECT, FINEP and CAPES-COFECUB (Project Ph598/08) for funding this study. Gisele A.B. Mello is indebted to CNPq for a Post-Graduation fellowship.

References

[1] C. Lamy, S. Rousseau, E.M. Belgsir, C. Coutanceau, J.-M. Léger, Electrochim. Acta 49 (2004) 3901–3908.
[2] G.A. Camara, T. Iwasita, J. Electroanal. Chem. 578 (2005) 315–321.
[3] G.A. Camara, R.B. de Lima, T. Iwasita, J. Electroanal. Chem. 585 (2005) 128–131.
[4] H. Wang, Z. Jusys, R.J. Behm, J. Power Sources 154 (2006) 351–359.
[5] M. Heinen, Z. Jusys, R.J. Behm, J. Phys. Chem. C 114 (2010) 9850–9864.
[6] S.C.S. Lai, S.E.F. Kleyn, V. Rosca, M.T.M. Koper, J. Phys. Chem. C 112 (2008) 19080–19087.
[7] J.A. Silva-Chong, O. Guillen-Villafuerte, J.L. Rodriguez, E. Pastor, J. Solid State Electrochem. 12 (2008) 517–522.
[8] G. Wu, R. Swaidan, G.F. Cui, J. Power Sources 172 (2007) 180–188.
[9] M.J.S. Farias, G.A. Camara, A.A. Tanaka, T. Iwasita, J. Electroanal. Chem. 600 (2007) 236–242.
[10] H. Wang, Z. Jusys, R.J. Behm, J. Appl. Electrochem. 36 (2006) 1187–1198.
[11] K.B. Kokoh, F. Hahn, E.M. Belgsir, C. Lamy, A.R. de Andrade, P. Olivi, A.J. Motheo, G. Tremiliosi-Filho, Electrochim. Acta 49 (2004) 2077–2083.
[12] J. Silva-Chong, E. Mendez, J.L. Rodriguez, M.C. Arevalo, E. Pastor, Electrochim. Acta 47 (2002) 1441–1449.
[13] E. Mendez, J.L. Rodriguez, M.C. Arevalo, E. Pastor, Langmuir 18 (2002) 763–772.
[14] E.P. Leão, M.J. Giz, G.A. Camara, G. Maia, Electrochim. Acta 56 (2011) 1337–1343.
[15] I.A. Rodrigues, F.C. Nart, J. Electroanal. Chem. 590 (2006) 145–151.
[16] J.P.I. de Souza, S.L. Queiroz, K. Bergamaski, E.R. Gonzalez, F.C. Nart, J. Phys. Chem. B 106 (2002) 9825–9830.
[17] T. Iwasita, F.C. Nart, Prog. Surf. Sci. 55 (1997) 271–340.
[18] G.A. Camara, R.B. de Lima, T. Iwasita, Electrochem. Commun. 6 (2004) 812–815.
[19] P. Glajchman, D.H. Wordell, M.J. Giz, G.A. Camara, J. Power Sources 195 (2010) 7221–7224.
[20] F. Richarz, B. Wohlmann, U. Vogel, H. Hoffschulz, K. Wandelt, Surf. Sci. 335 (1995) 361–371.
[21] S.S. Gupta, J. Datta, J. Electroanal. Chem. 594 (2006) 65–72.
[22] F.H.B. Lima, D. Profeti, W.H. Lizcano-Valbuena, E.A. Ticianelli, E.R. Gonzalez, J. Electroanal. Chem. 617 (2008) 121–129.
[23] R.B. de Lima, V. Paganin, T. Iwasita, W. Vielstich, Electrochim. Acta 49 (2003) 85–91.
[24] E. Pastor, S. González, A.J. Arvia, J. Electroanal. Chem. 395 (1995) 233–242.
[25] C.A. Martins, M.J. Giz, G.A. Camara, Electrochim. Acta 56 (2011) 4549–4553.
[26] R.G.C.S. Reis, C.A. Martins, G.A. Camara, Electrocatal. 1 (2010) 116–121.